7B.1 Measurements of Turbulence structure in the daytime convective boundary layer from a ground-based Doppler lidar

Marie Lothon*(1), Donald H. Lenschow(2), and Shane Mayor(2)

(1) Université de Toulouse, Laboratoire d'Aérologie - CNRS UMR 5560, Toulouse, France
(2) National Center for Atmospheric Research, Boulder, CO

1. INTRODUCTION

Recent developments in remote sensing technology now allow us to obtain simultaneous measurements of radial velocity throughout the convective boundary layer (CBL). Here we report on application of the NOAA High-Resolution Doppler Lidar (HRDL), deployed at the surface in a vertically-pointed mode, to measuring the spectra of vertical air velocity w throughout the CBL from $z \simeq 390$ m to near the CBL top z_i. The data were collected during the Lidars in Flat Terrain (LIFT) experiment (Cohn et al., 1998), carried out over nearly level farmland in central Illinois in July 1996. Previously, these data were used by Lothon et al. (2006) in a study of integral scales and two-point turbulence statistics in the CBL.

The HRDL system generates coherent infrared pulses at 2.0218 μm wavelength which are transmitted and received by a 0.2 m telescope at a pulse repetition rate of 200 s^{-1}. A beam-steering mechanism installed on the roof of the shipping container housing the lidar allowed pointing and scanning anywhere above the horizon. During LIFT, the laser generated 0.8 mJ pulses with a radial resolution of 30 m, and a minimum range (dead-zone) of about 390 m. Typically, the lidar was able to "see" several kilometers horizontally and, at the zenith, was always able to see through the top of the CBL. Changes in aerosol scattering led us to vary the number of pulses averaged together, and thus the temporal resolution (from one to a few seconds) on a daily basis.

Although the HRDL was used in various scanning modes during LIFT, a majority of the observations (110 out of over 160 hours) were with the laser beam pointing straight up, since a major focus of LIFT was to examine the vertical structure of w in a CBL. This takes advantage of the lidar's capability to obtain range-resolved radial measurements, from which a two-dimensional field of w can be obtained by use of Taylor's hypothesis; that is by assuming that the field of turbulence is "frozen" as it advects past the lidar.

The vertical time-height cross-sections are used to calculate spectra as a function of height. We then compare the observed spectra with previous analytical formulations by Kristensen et al. (1989) and discuss the differences.

*corresponding author address: Marie Lothon, Centre de Recherches Atmosphériques, 8 route de Lannemezan, 65300 Campistrous, France; *email*: lotm@aero.obs-mip.fr

2. MEAN STRUCTURE OF THE PBL

Table 1 summarizes the mean characteristics of the CBL for each case over the selected period of time (about 3 to 4 hours approximately centered in the middle of the day) that was chosen for analysis. The periods were selected on the basis of data continuity and quality, and stationarity of the CBL. On most of the days, fair-weather Cu formed by late morning, but some days showed absolutely no cloud. The cloud fraction χ above the lidar was estimated using a threshold on the HRDL backscatter. Two cases had a maximum of about 4/8; all other cases had $\chi < 4/8$.

The atmosphere was often hot and moist and it rained on 17 and 18 August. Profiles of the horizontal mean wind U were obtained from the wind profiler located at Sadorus, IL, about 5 km from the HRDL. The mean potential temperature and water vapour mixing ratio were estimated from radiosondes at the nearest time released about 5 km from the HRDL.

The CBL top z_i was determined from the height at which the increase in variance of the Doppler velocity over 1-minute segments first exceeded 0.7 m^2s^{-2} over a height increment of 30 m. That is, when the aerosol backscatter first becomes too weak to provide a measurable velocity and the signal is dominated by noise. Thus, we assume that z_i is a demarcation between a particulate-laden CBL and a relatively clean free troposphere. This criterion also identifies cloud base when fair-weather cumulus are growing out of the CBL top. This method did not work for one case (20 August), because two layers of aerosols were present with measurements of w in both. We used the CBL top given by a collocated profiler for that case. The estimates of the averaged z_i shown in Table 1 compare well with independent estimates from the nearby wind profilers and with the analyses of Cohn and Angevine (2000), Grimsdell and Angevine (1998), and Grimsdell and Angevine (2002). z_i ranges from 1000 to 1800 m over our 11 cases.

Table 1: Mean characteristics of the 11 LIFT cases considered here. θ_{v_m} and r_{v_m} are the mean virtual potential temperature and water vapour mixing ratio in the mixed layer, w_* is the convective velocity scale, u_* is the friction velocity, $\Delta\theta_v$ and $\Delta U = \sqrt{\Delta u^2 + \Delta v^2}$ are jumps across the inversion, γ is the lapse rate above the CBL, $\zeta = -z_i/L_o$, where L_o is the Monin-Obukhov length, χ is the cloud fraction, and l_w and λ_w are respectively the observed along-wind (transverse) integral scale and the wavelength λ_w at which the w energy density spectrum reaches its maximum, both evaluated at $z_i/2$ and normalized by z_i in the table. "/" indicates that $\Delta\theta_v$ was too small to be estimated.

Date of 1996	z_i m	U m s^{-1}	θ_{v_m} K	r_{v_m} g kg^{-1}	w_* m s^{-1}	u_* m s^{-1}	$\Delta\theta_v$ K	ΔU m s^{-1}	γ K km^{-1}	ζ	χ	l_w/z_i	λ_w/z_i
2 Aug	1590	3.0	299.8	9.8	1.58	0.16	1.16	1.0	4.7	407	0.47	0.14	0.85
4 Aug	1440	5.2	302.9	10.9	1.23	0.35	/	1.8	2.0	17	0.26	0.14	0.81
5 Aug	1190	8.6	306.7	14.7	1.34	0.52	1.86	5.8	2.4	7	0.28	0.13	0.78
6 Aug	1390	7.8	307.7	13.1	1.36	0.46	1.16	1.0	5.9	10	0.20	0.33	4.19
7 Aug	1270	5.6	308.7	15.6	1.29	0.39	0.35	2.2	1.8	14	0.28	0.25	2.33
10 Aug	1770	2.2	299.6	8.3	1.55	0.39	2.32	2.9	7.6	220	0.21	0.18	1.26
12 Aug	1720	4.8	300.8	10.7	1.56	0.19	1.16	1.1	2.6	37	0.41	0.29	1.79
16 Aug	1370	2.2	298.8	8.2	1.62	0.34	4.88	4.1	1.6	236	0.17	0.29	1.85
19 Aug	1280	7.2	304.1	11.8	1.55	0.19	3.95	2.9	1.0	9	0.21	0.24	2.33
20 Aug	960	6.8	305.5	14.8	1.14	0.43	1.63	3.1	1.2	8	0.05	0.18	1.46
21 Aug	1300	3.4	305.6	11.5	1.20	0.26	0.7	0.9	1.3	41	0.13	0.23	1.61

In Table 1, ΔU, $\Delta\theta_v$, and γ, where $\Delta(\ )$ refers to the jump across the inversion, characterize the entrainment zone and the stability of the free troposphere above, based on wind profiler and radiosonde measurements. The types of CBL taken into account range from no-shear to significantly sheared CBL, with a large distribution of mean wind from weak to moderate.

We also calculated the convective velocity scale w_* and the friction velocity u_* for scaling the spectra and dissipation of turbulence kinetic energy (TKE). For this, we used the momentum fluxes estimated from a weighted average of three ground stations deployed during the Flatland experiment (Militzer et al., 1995). The Monin-Obukhov length L_o was also estimated and used to calculate the instability criterion $\zeta = -z_i/L_o$.

Table 1 also displays the length scales that will be discussed later in conjunction with the w spectra: the integral scale l_w estimated from the autocorrelation of the w time series (along wind) and the wavelength λ_w for the maximum in the w spectrum. l_w is the characteristic scale over which the vertical velocity is significantly correlated with itself, which is a characteristic eddy size. λ_w is the characteristic scale of the turbulent energy production, which is more related to the distance between thermals in the CBL.

3. MODEL OF VERTICAL VELOCITY SPECTRA

While the spectra have fairly robust dependence on height within the surface layer (Kaimal et al. 1972), their evolution with height in the mixed layer is less well documented and less robust because of possible effects of processes at the CBL top such as entrainment and waves.

Kristensen et al. (1989; hereafter KLKC) postulate a general kinematic spectral model for an anisotropic horizontally homogeneous vertical velocity field:

$$\frac{S_w(k)}{\sigma_w^2} = \frac{l_w}{2\pi} \frac{1 + \frac{8}{3}\left(\frac{l_w k}{a(\mu)}\right)^{2\mu}}{\left\{1 + \left(\frac{l_w k}{a(\mu)}\right)^{2\mu}\right\}^{5/(6\mu)+1}}, \qquad (1)$$

where

$$a(\mu) = \pi \frac{\mu\Gamma\left(\frac{5}{6\mu}\right)}{\Gamma\left(\frac{1}{2\mu}\right)\Gamma\left(\frac{1}{3\mu}\right)}, \qquad (2)$$

l_w is the integral length scale, μ governs the curvature of the spectrum across the transition from negative to zero slope, and Γ is the gamma function. For $\mu = 1$ this model gives the Von Kàrmàn spectrum, and for $\mu = 0.5$ the Kaimal spectrum. In the KLKC model, the wavelength for which the spectrum reaches its maximum is

$$\lambda_w = \left\{\frac{5}{3}\sqrt{\mu^2 + \frac{6}{5}\mu + 1} - \left(\frac{5}{3}\mu + 1\right)\right\}^{1/(2\mu)} \frac{2\pi}{a(\mu)} l_w. \qquad (3)$$

So that λ_w is proportional to l_w, with a coefficient depending on μ.

The KLKC model also gives

$$\sigma_w^3 = a(\mu)^{-5/2}\left(\frac{\pi\alpha}{2}\right)^{3/2}\varepsilon l_w, \quad (4)$$

where ε is the TKE dissipation rate. Thus, substituting (3) in (4) we have:

$$\sigma_w^3 = b(\mu)\lambda_w\varepsilon, \quad (5)$$

where

$$b(\mu) = \frac{a(\mu)^{-5/2}\left(\frac{\pi\alpha}{2}\right)^{3/2}}{\left\{\frac{5}{3}\sqrt{\mu^2+\frac{6}{5}\mu+1}-\left(\frac{5}{3}\mu+1\right)\right\}^{1/(2\mu)}\frac{2\pi}{a(\mu)}}, \quad (6)$$

which links dissipation, energy and length scale.

4. OBSERVED SPECTRA

Figure 1 compares the spectra normalized with the square of the convective velocity w_*, for 6 out of the 11 cases considered in our study with the KLKC model for μ=0.5 (Kaimal spectrum) and μ=1.4. The observed spectra show considerable variability over the cases, with different shapes and different variation with height.

Usually the energy decreases with height, and the locations of the peaks and valleys show little change with height. Some cases have a decrease in energy with height for kz_i larger than a certain threshold near the start of the inertial subrange (5, 6, 7, 12, 19, 20 August) and others show energy decreasing with height for all kz_i (2, 4, 10, 16, 21 August). Four cases out of 11 show a variability of spectral energy with height that depends to a large extent on the wavenumber (5, 6, 19 and 20 August), with much smaller variability in the inertial subrange than at smaller wavenumbers. The variation of the spectral energy with height for all other cases is quite linear over the entire wavenumber range. The subset 5, 6, 19 and 20 August of the first set mentioned above are those with larger windspeed. Also note that 7 and 12 August have an intermediate behavior between these two classes, and they also have intermediate windspeed.

We calculated the modeled spectra (1) using the length scale l_w that solves (3) for our estimates of λ_w (rather than using the observed integral scales) and for different values of μ: μ=1 (Von Kàrmàn spectrum), μ=0.5 (Kaimal spectrum), for which the curvature around the maximum is less sharp, and μ=1.4 which is sharper than the Von Kàrmàn spectrum. The modeled spectra in Fig. 1 are plotted at the highest and lowest height where the velocity spectrum can be measured, while the observed spectra are shown over the whole probed PBL depth with a varying color scale.

μ=1.4 seems the best fit for almost all spectra. As will be discussed later, this is also consistent with Figure 3 where μ=1.4 gives a coefficient between λ_w and l_w which better fits the observations. August 12, 16 and 19 are cases for which the modeled spectra do not fit well, because of singular behavior of the observed spectra, with energy production up to relatively large scales and a precipitous drop at still larger scales.

5. OBSERVED CHARACTERISTIC LENGTH SCALES

For each day and each range, integral scales and spectra of the vertical velocity w are computed for all of the cases. We assume Taylor's hypothesis of frozen turbulence advected by the mean wind.

The estimates of the integral scales l_w discussed in detail in Lothon et al. (2006) are obtained from the autocorrelation function of w at each height. l_w/z_i at $z_* = z/z_i$=0.5 is displayed in Table 1.

The estimates of λ_w are based on a fit of the spectra to a simpler model than explained above, which gives estimates that are more continuous with height than those obtained directly from finding the position of the energy maximum. However, this approach can smear out the absolute spectral maximum for spectra with several peaks. The simple model used to estimate the spectral wavelength is of the form:

$$kS(k,z_*) = \frac{a(z_*)k}{1+\left(\frac{k}{k_0(z_*)}\right)^{5/3}}, \quad (7)$$

where a and k_0 are determined from a least-squares fit to the observed spectrum, $z_* = z/z_i$, and

$$\lambda_{w_f}(z_*) = \frac{2\pi}{k_0(z_*)}. \quad (8)$$

In Fig. 2, the vertical profiles of our estimates of λ_w are compared with the relationship found by Caughey and Palmer (1979) for the region $0.1 < z_* < 1$:

$$\frac{\lambda_w}{z_i} = 1.8\left(1-e^{-4z_*}-0.0003e^{8z_*}\right). \quad (9)$$

$\lambda_w \simeq$1.8 through most of the middle part of the CBL. Four cases show profiles of λ_w/z_i close to the prediction: 10, 16, 20 and 21 August. 2, 4, 5 and 12 August show smaller λ_w/z_i and 6, 7 and 19 August show larger λ_w/z_i. The profiles of the wavelength of the absolute maximum spectral density, which typically are constant with height through many successive levels, demonstrate the repeatability of the peaks throughout much of the CBL, which is consistent with the measured coherence being larger than predicted for isotropic turbulence with the observed integral length scale (Lothon et al. 2006).

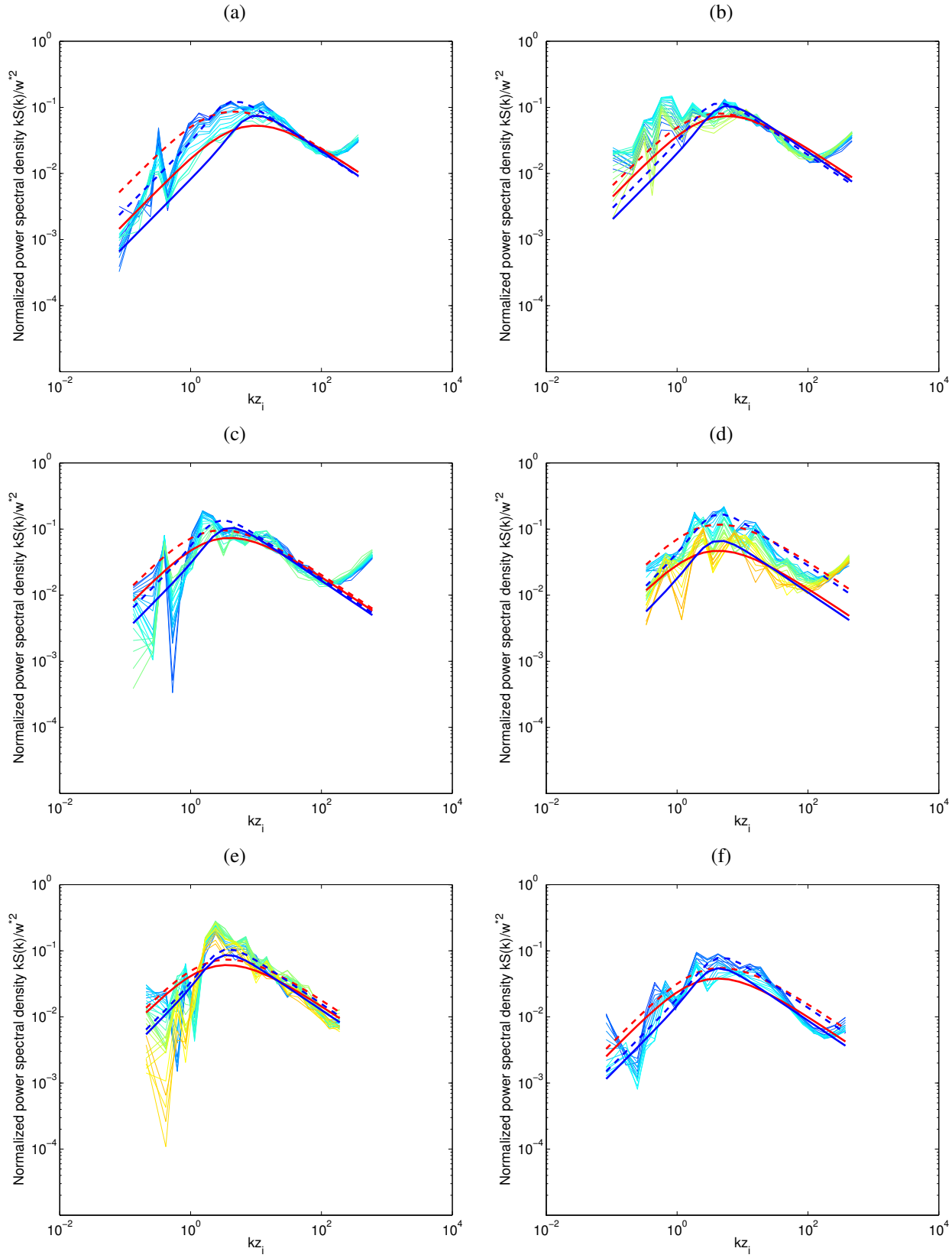

Figure 1: *Normalized spectral density of w multiplied by wavenumber ($kS(k)/w_*^2$) as a function of kz_i for 6 days in August 1996: (a) 5, (b) 6, (c) 7, (d) 10, (e) 12, (f) 20 August. Levels vary from about 0.25 z_i (dark blue) to about 0.75 z_i (yellow to orange) every 30 m. The smooth red and blue lines are the modeled spectra given in (1) for respectively μ=0.5 and μ=1.4. They are plotted for the highest (solid) and lowest (dashed) levels observed.*

Figure 3 displays λ_w/z_i as a function of l_w/z_i as observed by the HRDL at $z_* = z_i/2$. We find a smaller slope than predicted by the theory, for all the values of μ considered here. This can be linked to the departures of the observed spectra from the model.

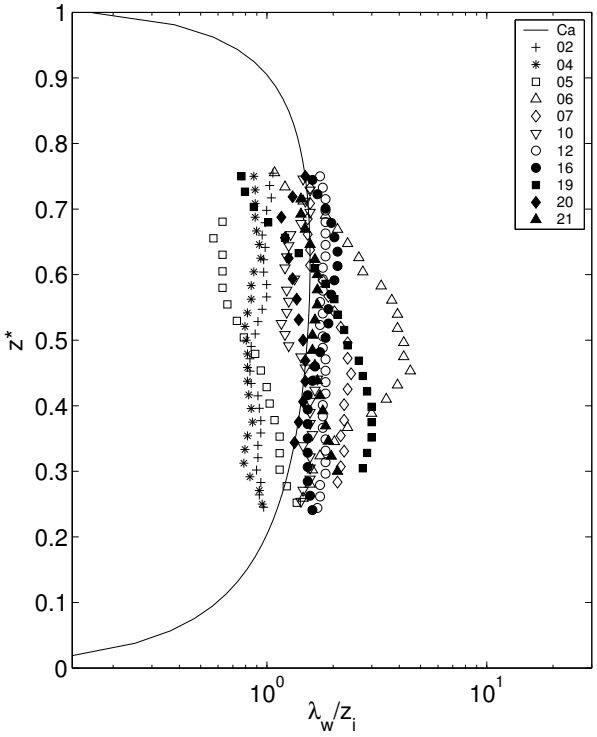

Figure 2: *Profiles of the wavelength λ_w of maximum spectral density of w, normalized by z_i for the 11 cases. Solid line is the profile found by Caughey and Palmer (1979) (equation 9).*

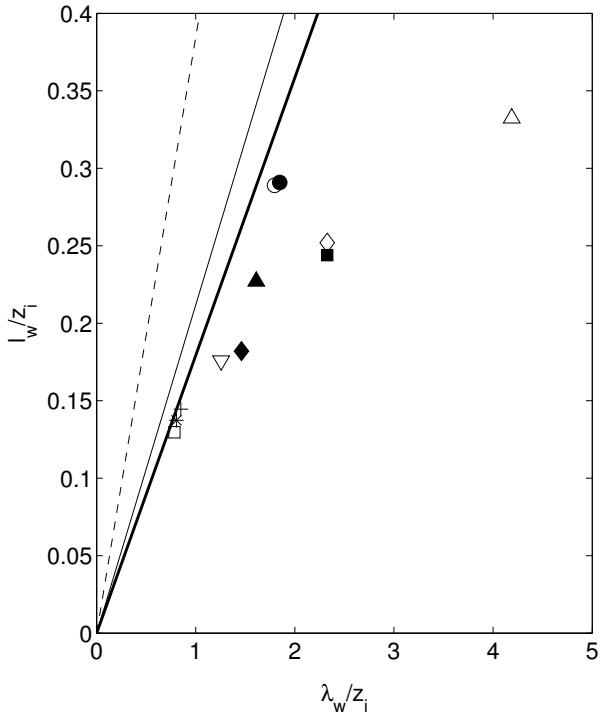

Figure 3: *Along wind integral scale of vertical velocity at $z_i/2$ (Lothon et al 2006) as a function of λ_{w_f} at $z_i/2$ for the 11 cases. Symbols are the same as in Fig. 2. The solid and dashed lines are the theoretical relationship for respectively μ=1 and μ=0.5. The thick solid line is for μ=1.4*

6. DISSIPATION

Dissipation rates ε are deduced from the inertial subrange of the spectra with Kolmogorov's hypothesis using a Kolmogorov constant of 0.52 over a range of $30 < kz_i < 80$. Figure 4 displays the profiles of TKE dissipation normalized by buoyancy for all cases. We can see that they show some significant scatter with $\overline{\varepsilon} z_i/w_*^3$ = 0.3 $\pm$ 0.1, where $\overline{\varepsilon}$ is an average over all cases and height.

We would expect the normalized dissipation to be somewhat more than 0.4 for an entrainment ratio A equal to 0.2, with

$$A = \frac{-\langle w\theta_v \rangle_{z_i}}{\langle w\theta_v \rangle_0}. \qquad (10)$$

where $\langle w\theta \rangle_{z_i}$ is the buoyancy flux at z_i and $\langle w\theta \rangle_0$ is the flux at the surface. Our results indicate that the entrainment flux may be less than this (or larger in modulus). The large scatter in the dissipation profiles likely results from a combination of shear production both near the surface and near the top of the CBL, and a varying ratio of entrainment to surface buoyancy flux. We can actually use the normalized dissipation along with a model of the turbulence kinetic energy (TKE) budget to estimate A. Using the TKE model of Lenschow and Stankov (1974), along with the mixed-layer growth model of Tennekes (1973) and a parameterization from Mahrt and Lenschow (1976) for the contribution of shear production across the CBL top, we find that A is larger than the commonly-used value of 0.2, and varies considerably from day to day.

Figure 5 displays observed σ_w^3 as a function of estimates of $\varepsilon\lambda_w$ on logarithmic scales. We observe the 1-to-1 slope predicted in (5), but the observed proportionality coefficient is larger than $b(\mu)$ calculated from (5) whatever μ is used. ($b(1)$=0.32 and $b(0.5)$=0.25). Indeed, $b(\mu)$ is maximum at μ=1.4, with $b(1.4)$=0.33, and we observe $b = 0.42$.

Consistent with the variability of the spectra observed with height in the inertial subrange, ε decreases with height in most cases and especially for the set of cases with lighter mean wind.

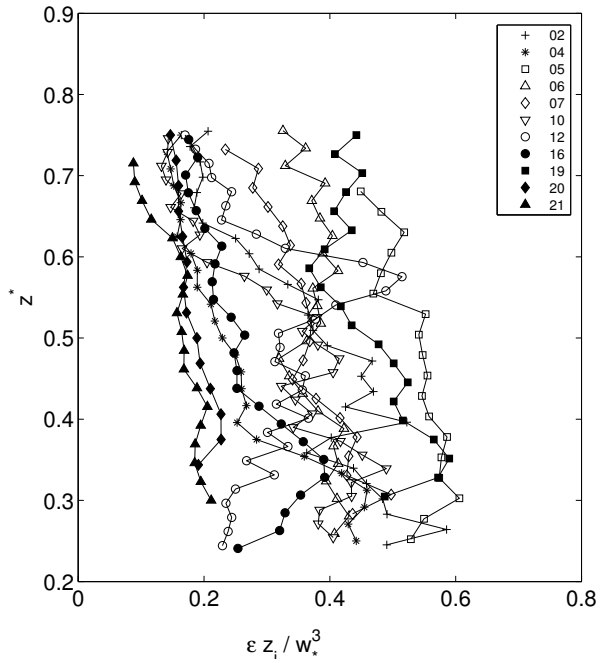

Figure 4: *Profiles of the normalized dissipation rate for each case.*

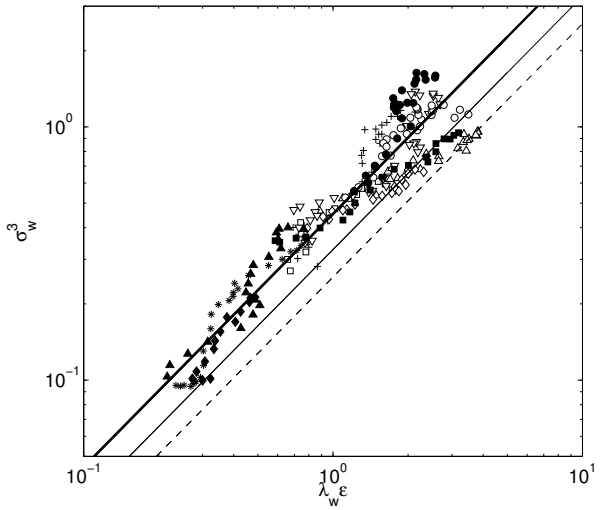

Figure 5: σ_w^3 *as a function of* $\lambda_w\varepsilon$ *for all cases and at all levels between about 0.25* z_i *and 0.75* z_i*. Thick solid line is a linear least square fit, thin solid line is the theoretical slope for* $\mu = 1$ *and the dashed line for* $\mu = 0.5$*.*

7. BEHAVIOR OF w SPECTRA AT SMALL WAVENUMBERS

In the mixed layer, the inertial subrange spectral region can be collapsed onto a single curve by the normalization (Kaimal et al. 1976)

$$\frac{kS(k)}{w_*^2\psi_\varepsilon^{2/3}} = \frac{kS(k)}{(\varepsilon z_i)^{2/3}} = \frac{4}{3}\alpha(kz_i)^{-2/3}, \qquad (11)$$

where

$$\psi_\varepsilon = \frac{\varepsilon z_i}{w_*^3}. \qquad (12)$$

Since ε is determined from the power spectrum in the inertial subrange, this law fits the observed spectra at the logarithmic mean of the range over which the estimates were computed. Some cases show a slope in the inertial subrange significantly steeper than $-2/3$, that usually gets closer to $-2/3$ for increasing z_*. We do not know why.

Figures 6 show the normalized spectra $\frac{kS(k)}{w_*^2\psi_\varepsilon^{2/3}}$ observed at respectively z_*=0.35 for all 11 cases.

Fig. 7 displays the averaged $\frac{kS(k)}{w_*^2\psi_\varepsilon^{2/3}}$ over $kz_i \in [0.1, 1]$ and over altitude as a function of shear across the CBL top. The shear is calculated using the UHF profiler data at Montecello, collocated with the HRDL lidar, and at Sadorus—5 km away—for cases for which there were no data from the first profiler (2, 7, 20 and 21 August). Fig. 7 seems to show lower energy of the spectra at small wavenumbers as the shear increases. However, the limited number of cases on which this is based (only two cases with large shear—6 and 20 August) make this only a tentative conclusion.

One possibility for why this may be the case is based on the large-eddy simulation results of Conzemius and Fedorovich (2006) who found that the bulk Richardson number Ri_b remains constant within the entrainment zone. To keep the Richardson number constant, larger shear must be associated with a larger jump in virtual potential temperature $\Delta\theta_v$, which may retard wave propagation through the entrainment zone.

8. SUMMARY OF THE RESULTS AND CONCLUDING REMARKS

The w spectra observed with the HRDL throughout the mixed layer revealed a significant consistency of their peaks throughout the depth of the PBL, in agreement with the large coherence found over the vertical by Lothon et al. (2006). But they also showed large case-to-case variability, both in the location of the spectral maximum, and in the shapes of the spectra in the energy-containing region. This makes it difficult to develop a generalized model of the w spectra, and indeed, we found that existing models do not characterize the w spectra very well.

Here we used the KLKC model for comparison, with a parameter μ that governs the curvature of the spectrum. We find that the spectra are more peaked than predicted by e. g. the von Kàrmàn ($\mu = 1$) or the Kaimal ($\mu = 0.5$) spectra; $\mu = 1.4$ seems a better fit to our observations.

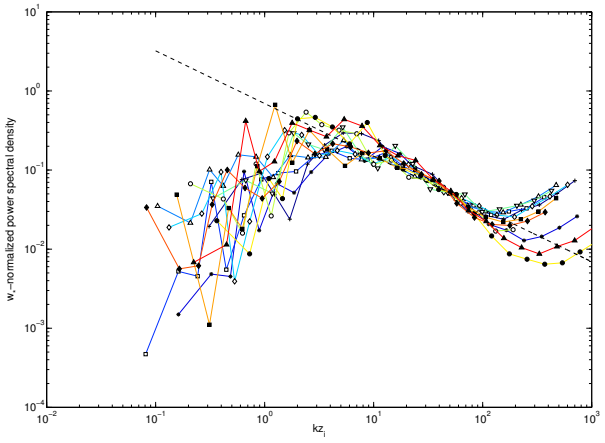

Figure 6: *Power density spectra multiplied by wavenumber and normalized by* $w_*^2\psi_\varepsilon^{2/3}$ $(kS(k)/(w_*^2\psi_\varepsilon^{2/3}))$ *as a function of* kz_i *at* z_**=0.35 for the 11 cases.*

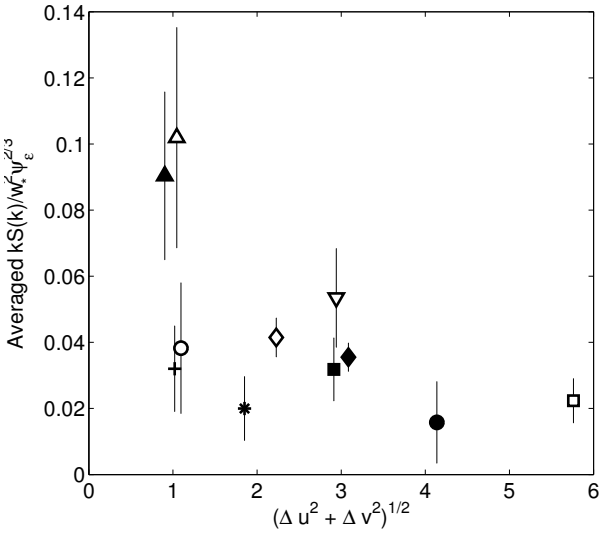

Figure 7: *Averaged value of* $\frac{kS(k)}{w_*^2\psi_\varepsilon^{2/3}}$ *over* $kz_i \in [0.1,1]$ *and over altitude as a function of* $\sqrt{\Delta u^2+\Delta v^2}$*, averaged over the considered time period before the calculation of shear (*Δu *and* Δv *are the differences in wind components u and v between just above the CBL top* $(z=z_i+z_i/10)$ *and their average within the depth of the CBL). Each symbols denotes a different case and the legend is the same as for Fig. 2.*

We find a strong correlation between the wavelength of the maximum of $kS(k)$ and the integral scale, but with the ratio λ_w/l_w larger than predicted.

The larger the mean wind, the larger the difference between large and small wavenumbers in spectral variability with height. Also, we find a larger contribution at low wavenumbers for smaller shear across the inversion, which we believe is a result of differences in dynamical processes associated with inversion strength.

Acknowledgements

The LIFT project was funded by the NCAR Atmospheric Technology Division Director's Office and the Department of Energy/OAGR. This work was made possible by support provided by the MMM and EOL Divisions of NCAR. The first author is supported by CNRS-INSU, France.

REFERENCES

Caughey, S. J. and S. G. Palmer, 1979: Some aspects of turbulence structure through the depth of the convective boundary layer, *Quart. J. Roy. Meteorol. Soc.*, **105**, 811–827.

Cohn, S. A. and W. M. Angevine, 2000: Boundary layer height and entrainment zone thickness measured by lidars and wind-profiling radars, *J. Appl. Meteorol.*, **39**, 1233–1247.

Cohn, S. A., S. D. Mayor, T. M. Grund, T. M. Weckwerth, and C. Sneff, 1998: The Lidars in Flat Terrain experiment LIFT, *Bull. Amer. Meteorol. Soc.*, **79**, 1329–1343.

Conzemius, R. J. and E. Fedorovich, 2006: Dynamics of sheared convective boundary layer entrainment. textscPart I: Methodology background and large-eddy simulations, *J. Atmos. Sci.*, **63**, 1151–1178.

Grimsdell, A. W. and W. M. Angevine, 1998: Convective boundary layer height measurement with wind profilers and comparison to cloud base, *J. Atmos. Oceanic Technol.*, **15**, 1331–1338.

—, 2002: Observations of the afternoon transition of the convective boundary layer, *J. Appl. Meteorol.*, **41**, 3–11.

Kaimal, J. C., J. C. Wyngaard, and O. R. Coté, 1972: Spectral characteristics of surface layer turbulence, *Q. J. R. Meteorol. Soc.*, **98**, 653–689.

Kaimal, J. C., J. C. Wyngaard, D. A. Haugen, O. R. Coté, and Y. Izumi, 1976: Turbulence structure in the convective boundary layer, *J. Atmos. Sci.*, **33**, 2152–2169.

Kristensen, L., D. H. Lenschow, P. Kirkegaard, and M. Courtney, 1989: The spectral velocity tensor for homogeneous boundary layer turbulence, *Boundary-Layer Meteorol.*, **47**, 149–193.

Lenschow, D. H. and B. B. Stankov, 1974: Model of the height variation of the turbulence kinetic energy budget in the unstable planetary boundary layer, *J. Atmos. Sci.*, **31**, 465–474.

Lothon, M., D. H. Lenschow, and S. Mayor, 2006: Coherence and scale of vertical velocity in the convective boundary-layer, *Boundary-Layer Meteor.*, **121**, 521–536.

Mahrt, L. and D. H. Lenschow, 1976: Growth dynamics of the convective mixed layer, *J. Atmos. Sci.*, **33, 41-51**.

Militzer, J. M., M. C. Michaelis, S. R. Semmer, K. S. Norris, T. W. Horst, S. P. Oncley, A. C. Delany, and F. V. Brock, 1995: Development of the prototype pamiii/fluxpam surface meteorological station, *Proceedings of the 9th Symposium on Meteorological Observations and Instrumentation, Amer. Meteorol. Soc., Boston*, pp. 490–494.

Tennekes, H., 1973: A model for the dynamics of the inversion above a convective boundary layer, *J. Atmos. Sci.*, **30**, 538–567.